Desalination and Water Treatment
www.deswater.com
doi: 10.5004/dwt.2019.24308

161 (2019) 293–303
September

Removal of sulfate from aqueous solution by magnetic chitosan microspheres

Zishun Tian[a], Tao Feng[a,b,*], Guodong Yang[a], Tingting Zhao[a], Li Wang[c]

[a]*College of Resources and Environmental Engineering, Wuhan University of Science and Technology, Wuhan 430081, China, Tel. +86 27 68862880; emails: fengtaowhu@163.com (T. Feng), 781779196@qq.com (Z. Tian), 416982807@qq.com (G. Yang), ttzhaowust@163.com (T. Zhao)*
[b]*Hubei Key Laboratory for Efficient Utilization and Agglomeration of Metallurgic Mineral Resources, Wuhan University of Science and Technology, Wuhan 430081, China*
[c]*Research Center for Environmental Pollution Control and Repair with Green Technology, Wuhan University of Science and Technology, Wuhan 430081, China, Tel. +86 27 68862885; email: wanglijohn@163.com*

Received 17 September 2018; Accepted 20 April 2019

ABSTRACT

The magnetic chitosan microspheres (Fe_3O_4/CS) were prepared by inverse suspension cross-linking and characterized by scanning electron microscope, optical micrographs, Fourier transform infrared spectrophotometer, and X-ray diffraction. They were employed as the adsorbents for the removal of sulfate from the aqueous solutions in the batch system. The magnetic material (Fe_3O_4) used in the preparation of the magnetic chitosan microspheres was prepared by precipitation from $FeCl_2$ and $FeCl_3$ solutions in the basic medium. The experimental results showed that Fe_3O_4/CS was an excellent adsorbent for the removal of sulfate with an adsorption capacity of 256.41 mg g^{-1}. Equilibrium isotherm study showed a good agreement with the Langmuir isotherm equation for the monolayer adsorption process, while the adsorption process can be well described by the second-order kinetic model and the Dubinin–Radushkevich isotherm further confirmed the presence of physical adsorption forces.

Keywords: Chitosan; Magnetic microspheres; Adsorption; Sulfate

1. Introduction

As a common contaminant, sulfate could be easily found in drinking water, surface water, groundwater, domestic sewage and industrial wastewater [1]. Among them, industrial wastewater is regarded as the main source for most anthropogenic emissions of sulfate into the environment. The content of sulfate in the domestic sewage was typically between 20 and 500 mg L^{-1}, while certain industrial effluents may contain several thousands of milligrams per liter [2]. A small amount of sulfate in water has no effect on human health; however, it may cause diarrhea, dehydration and gastrointestinal dysfunction when the sulfate content exceeds the limit. Besides that, high sulfate concentrations can unbalance the natural sulfur cycle and the accumulation of sulfate-rich sediments in lakes, rivers and sea may cause the release of toxic sulfides that can provoke damages to the environment [3].

Over the years, a variety of techniques have been developed for the removal of dissolved sulfate, including precipitation, crystallization, adsorption, electrochemistry, ion exchange, etc. [4–8]. Among these techniques, adsorption has been widely studied since it is a kind of economic, easy operating, low cost and less pollution method. Nowadays, various adsorbents, such as calcined Mg–Fe layered double hydroxides [9], granular ferric hydroxide [10], palygorskite [11], and modified nature polymers [12], have been used for the removal of sulfate. Chitosan

* Corresponding author.

(CS), the deacetylation product of natural chitin, has been widespread concerned due to its excellent biodegradability and biocompatibility and the characteristics of nontoxicity and environmentally friendly. So, a large amount of studies focus on chitosan-based adsorbents, flocculants and their applications in water treatment [13,14]. The existence of amino and hydroxyl in its structure provide a good adsorption performance for many anions, such as F^-, ClO_4^- and NO_3^- [15–17]. However, the studies on sulfate sorption onto chitosan and its derivatives are very few.

Although the mechanical strength, chemical stability and hydrophilicity could be improved by modification, such as cross-linking, sometimes the chitosan is still difficult to be separated from the water rapidly after adsorbed. On the other hand, some of the contaminants need to be recovered because of its precious features. So it is needed to seek techniques for separation of the adsorbents from the water efficiently. Recently, magnetic separation technologies have been applied into the field of wastewater treatment. These magnetic substances could be separated from the water rapidly and efficiently by using the external magnetic field since magnetic forces were much greater than gravitation [18]. A quaternary ammonium salt modified chitosan magnetic composite adsorbent (CS-CTA-MCM) was prepared by combination of Fe_3O_4 nanoparticles and it can adsorb both methyl orange and chromium from their aqueous mixtures efficiently [19].

In this study, the magnetic-chitosan particles (Fe_3O_4/CS) were prepared and employed to remove sulfate from the solution. The inverse suspension cross-linking technology was used for the production of Fe_3O_4/CS, and PEG_{2000} was used as the porogen while epichlorohydrin (ECH) was used as a cross-linker. The effects of the Fe_3O_4/chitosan ratio, pH, initial concentration, contact time and dosage on the adsorption were investigated. The characterization, adsorption kinetics and isotherms on Fe_3O_4/CS were used to better understand the adsorption characteristics of sulfate.

2. Materials and methods

2.1. Reagents

Chitosan with its deacetylation degree of 90% was supplied by Zhejiang Ocean Biochemical Company (Taizhou, China). Analytical grade K_2SO_4 was used as the source of sulfate anions. $FeCl_2{\cdot}7H_2O$, $FeCl_3{\cdot}6H_2O$, NaOH, HCl, liquid paraffin, glacial acetic acid, PEG_{2000}, Span-80, formaldehyde and epichlorohydrin were also of grade. Distilled water was used throughout the study.

2.2. Instruments

DJ1C Motor agitator (Shanghai Jingfeng instrument co., LTD., China), Thermostat water bath cauldron (Jiangsu Jintan XinYiJia Instrument Factory, China), HY-6 double multipurpose speed oscillator (Jiangsu Jintan Ronghua Instrument Manufacture Co., LTD., China), ISC-90 (Dionex Co., USA).

2.3. Preparation of magnetic Fe_3O_4 nanoparticles

Magnetic Fe_3O_4 nanoparticles were prepared by co-precipitation method [20]. First, 4.9703 g $FeCl_2{\cdot}7H_2O$ and 6.7575 g $FeCl_3{\cdot}6H_2O$ were dissolved into the distilled water to prepare a 0.5 mol L^{-1} iron-contained solution, respectively. Then, 20 mL of Fe^{2+} solution, 40 mL of Fe^{3+} solution and 200 mL 3 mol L^{-1} sodium hydroxide solution were added to a flask in order. The mixed liquor was stirred violently at 323.15 K for 40 min. Afterwards, the sediment was repeatedly washed with ethyl alcohol and distilled water to remove unreacted chemicals. Finally, the wet magnetic particles were obtained using magnet and dried in a vacuum drier. The reaction involved was shown in Eq. (1).

$$FeCl_2 \cdot 7H_2O + 2FeCl_3 \cdot 6H_2O + 8NaOH \rightarrow Fe_3O_4 \downarrow + 8NaCl + 23H_2O \quad (1)$$

2.4. Preparation of Fe_3O_4/CS

In a 2% (v/v) aqueous acetic acid solution, 4 g pure chitosan, 1.6 g PEG_{2000} and a certain amount of magnetic Fe_3O_4 nanoparticles were dissolved to prepare a mixing solution. Then, liquid paraffin and a small amount of Span-80 were added to the chitosan mixing solution. The mixed liquor was stirred violently at 313.15 K for 1 h until it was emulsified, then added 30 mL formaldehyde and stirred for 2 h. Afterwards, the wet microspheres were washed, filtered and immersed in a certain amount of 0.1% (v/v) cross-linking agent solution at 343.15 K for 4 h. Finally, the wet microspheres were washed repeatedly with distilled water until it became neutral and dried in vacuum condition to get cross-linked magnetic chitosan (Fe_3O_4/CS).

2.5. Characterization

2.5.1. Morphology

The morphological characterization of the samples was carried out with a scanning electron microscope (SEM) and the optical micrographs (OM). All the samples were fixed on the conductive adhesive and plated with gold, and then observed by Nova 400 Nano SEM. The cross-linked magnetic chitosan swelled up in water for 24 h before observation in OM.

2.5.2. Functional groups

FTIR spectra were recorded before and after processing of the chitosan polymers into sphere form for observing the functional groups of the chitosan microspheres. The samples were thoroughly mixed with KBr at the ratio of 1:100 (w/w) and then pressed into tablet form. FTIR spectra were recorded with KBr pellets on Nicolet-360 FT-IR spectrometer in the wave range of 4,000–400 cm^{-1}.

2.5.3. Crystal structure

The crystalline structure of the samples was observed by X-ray diffraction (XRD). The patterns of XRD were recorded using CuKα radiation of wavelength 0.1544 nm on a type of D/MAX-IIIAX diffractometer operating at 40 kV and 50 mA. The powder diffraction patterns were obtained between 5° and 40°.

2.6. Batch adsorption studies

Batch adsorption studies were carried out in stopper conical flasks containing 50 mL sulfate solution and a

little modified chitosan powder. The reaction mixture was agitated in double multi-purpose speed oscillator (120 rpm, 303.15 K) for desired time followed by filtration. The sulfate content left in the supernatant solution after adsorption process was analyzed immediately by ion chromatography method. The adsorption capacity of the adsorbents and the removal rate of sulfate ions are calculated from the following equations:

$$Q = \frac{\left(C_0 - C\right)}{1{,}000m} \times V \tag{2}$$

$$\eta = \frac{C_0 - C}{C_0} \times 100\% \tag{3}$$

where C_0, C represent the concentration (mg L^{-1}) of sulfate in solution before and after adsorption, respectively, V is the volume of sulfate solution (50 mL), m is the mass (g) of dry microspheres.

3. Results and discussion

3.1. Characterization

3.1.1. Morphology study

SEM micrographs of pure chitosan microspheres (a), Fe_3O_4/CS (b, c), OM micrographs of Fe_3O_4/CS (d) and recycled Fe_3O_4/CS after adsorption (e, f) are shown in Fig. 1. Compared with the pure chitosan microspheres, the surfaces of Fe_3O_4/CS were rough. We can see the porous microstructure clearly, which may obviously increase the adsorption capacity. Fig. 1d shows an optical micrograph of magnetic chitosan microspheres, it can be seen that the distribution of Fe_3O_4 particles in the microspheres. According to the SEM images in Fig. 1, the particles were micron-sized and spheroidal, and the sizes were in the range of 100 to 250 μm. As can be seen from Figs. 1e and f, after five batch adsorption cycles, the morphology of Fe_3O_4/CS did not change significantly, the microspheres were still well shaped and regular, which indicates that the Fe_3O_4/CS microspheres had a certain strength in the adsorption process.

3.1.2. FTIR analysis

The FTIR results are shown in Fig. 2, as can be seen that peaks at 579 cm^{-1} in Fig. 2a attribute to the Fe–O bond vibration of Fe_3O_4 [21]. For pure chitosan (b), the predominant peaks at 3,433, 2,922, 1,637, 1,395, and 1,072 cm^{-1} are indicative of –OH and –NH stretching vibrations, C–H stretching vibrations, –NH bending vibration in $–NH_2$ and –C=O stretching vibrations in acetylamino, –NH deformation vibration in $–NH_2$, and –CO stretching vibration, respectively [16].

The characteristic peaks at 1,385 and 1,620 cm^{-1} (Fig. 2c) indicated that cross-linking reaction took place between the aldehyde group of cross-linking agent and the amine groups of CS. Due to the coordination between the –OH and $–NH_2$ of CS and Fe_3O_4, some displacements could be seen in the characteristic absorption peaks [22]. For example, peaks at 671 cm^{-1} in Fig. 2c attribute to the characteristic absorption peaks of Fe_3O_4. Compared with the pure chitosan, the peaks at 1,072 cm^{-1} moved to 1,115 cm^{-1}, indicating that Fe atoms coordinated with O atoms of –OH. At the same time, the peaks at 3,433 cm^{-1} moved to 3,430 cm^{-1}, which indicated that the coordination reaction also took place between Fe atoms and the lone pair electrons of N atoms of $–NH_2$.

Fig. 2d shows the infrared spectrum of Fe_3O_4/CS after adsorption. It could be seen that peaks at 1,551 cm^{-1} became wider and weaker, which may indicate that the derivative reaction took place on the amidogen of CS. Furthermore, the peaks at 1,637 cm^{-1} also became weaker indicated that the acylamino of CS may join in the adsorption process. The whole structure of the infrared spectrum had little change, which indicated that the adsorption process was closer to physical adsorption.

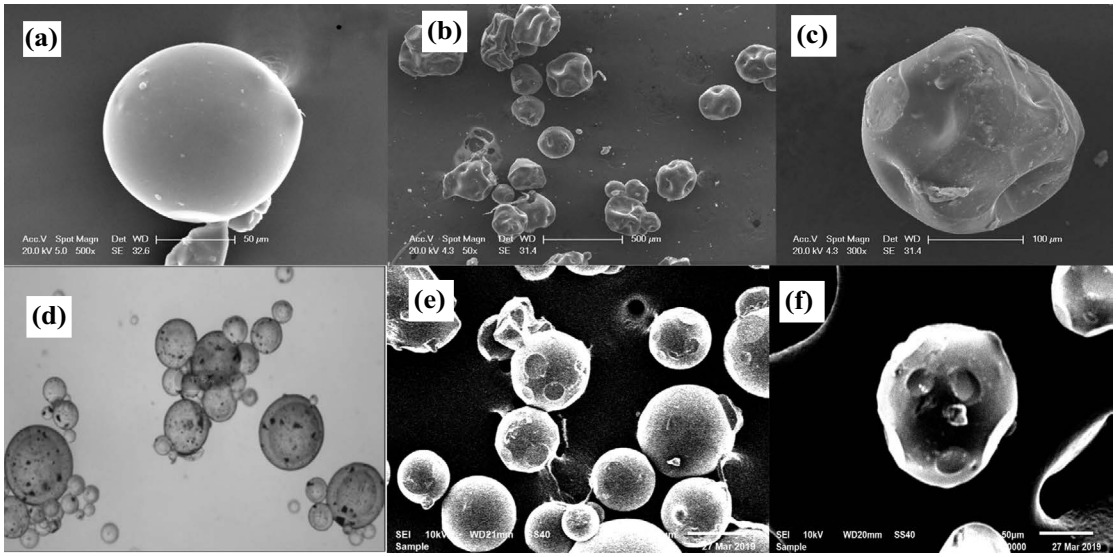

Fig. 1. SEM micrographs of pure chitosan microspheres (a), Fe_3O_4/CS (b, c), OM micrographs of Fe_3O_4/CS (d) and recycled Fe_3O_4/CS after adsorption (e, f).

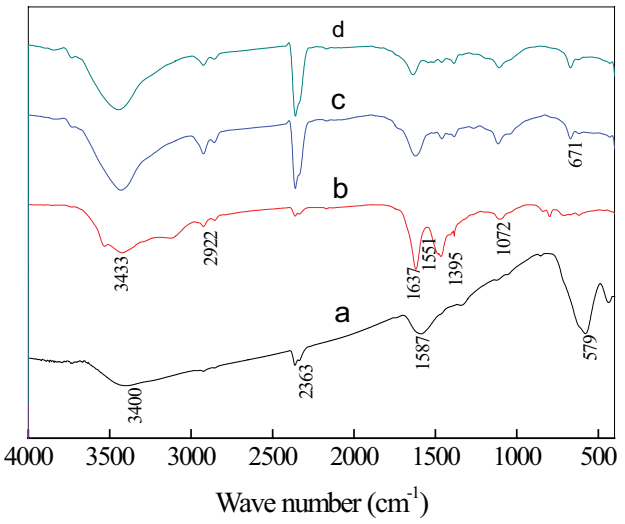

Fig. 2. FTIR spectra of Fe_3O_4 (a), pure chitosan (b), Fe_3O_4/CS (c), and Fe_3O_4/CS adsorbed sulfate (d).

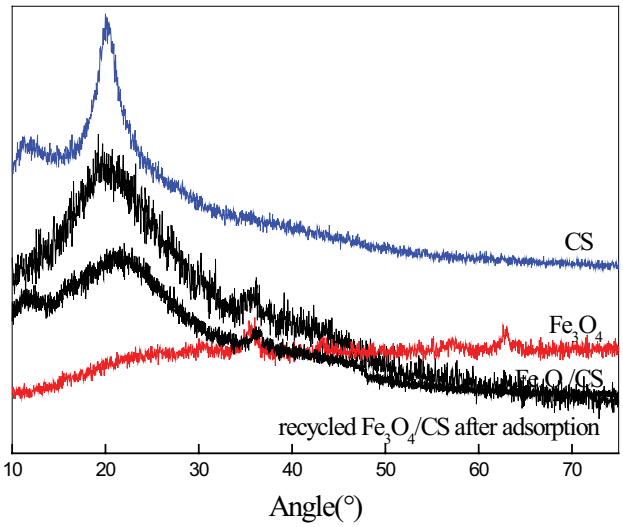

Fig. 3. XRD spectra of the microspheres.

3.1.3. XRD analysis

Fig. 3 shows the XRD pattern of CS, Fe_3O_4, Fe_3O_4/CS and recycled Fe_3O_4/CS after adsorption. It can been seen that the pure chitosan had strong diffraction peaks at 2θ = 12.71° and 20.16°, while the diffraction peaks of Fe_3O_4/CS at 12.71° almost disappeared after modification. The diffraction peaks became obviously weaker and shifted to 19.70°. At the same time, the amorphous area increased apparently. These changes indicated that the crystallinity of Fe_3O_4/CS decreased compared with the CS. Besides, the main diffraction peaks of Fe_3O_4/CS at 2θ = 36.01°and 62.61° in the XRD pattern were in accordance with that of Fe_3O_4, indicating that Fe_3O_4/CS is composed of chitosan and Fe_3O_4, whose crystallinity was not affected by Fe_3O_4. And after five batch adsorption cycles, there were no obvious changes in the XRD pattern of recycled Fe_3O_4/CS.

Through the above characterization analyses, the mechanism of the preparation of modified chitosan can be expressed in Fig. 4.

3.2. Effect of reaction conditions on the sulfate adsorption

3.2.1. Effect of the Fe_3O_4/chitosan ratio

In order to determine the optimal mass ratio of Fe_3O_4 and chitosan, a certain amount of magnetic Fe_3O_4 nanoparticles were added to prepare the different mass ratio of Fe_3O_4/CS. The Fe_3O_4/chitosan ratio varied in the range of 0.00:4 to 0.40:4 (g/g). Therefore, the adsorption experiments were carried out with 50 mL, 600 mg L^{-1} of sulfate solutions at 303.15 K, and 0.05 g cross-linked magnetic chitosan were weighed and added to solutions under oscillating for 3h. As shown in Fig. 5a, the adsorption capacity of sulfate firstly goes down and then goes up, when achieving the

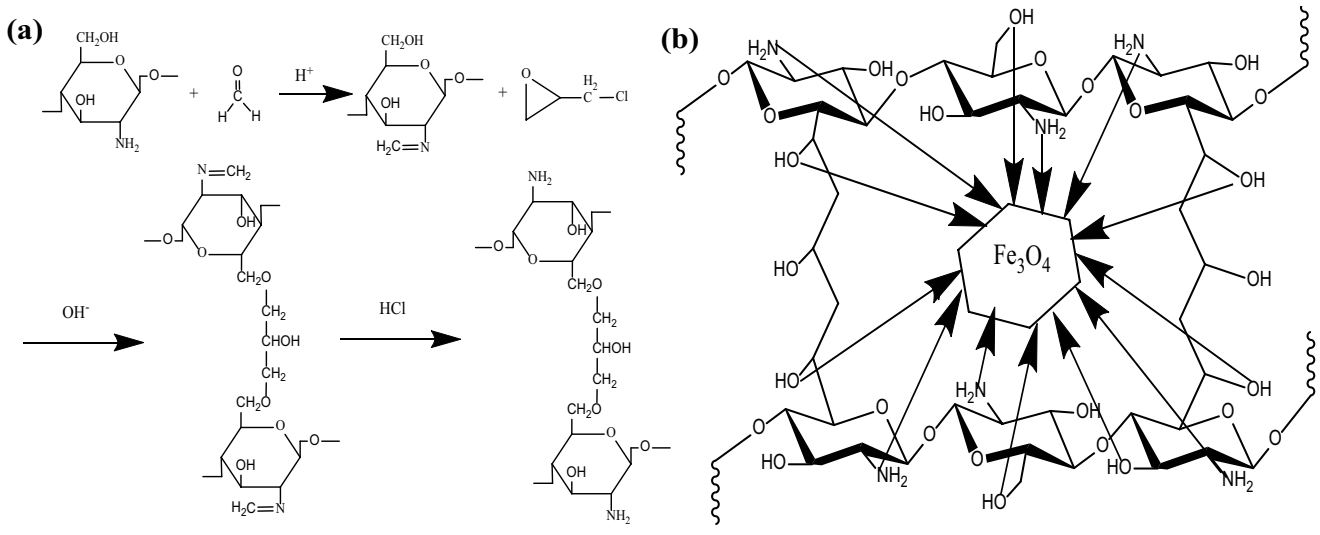

Fig. 4. Cross-linking mechanism of formaldehyde and ECH (a) and interaction mechanism of Fe_3O_4/CS complex (b).

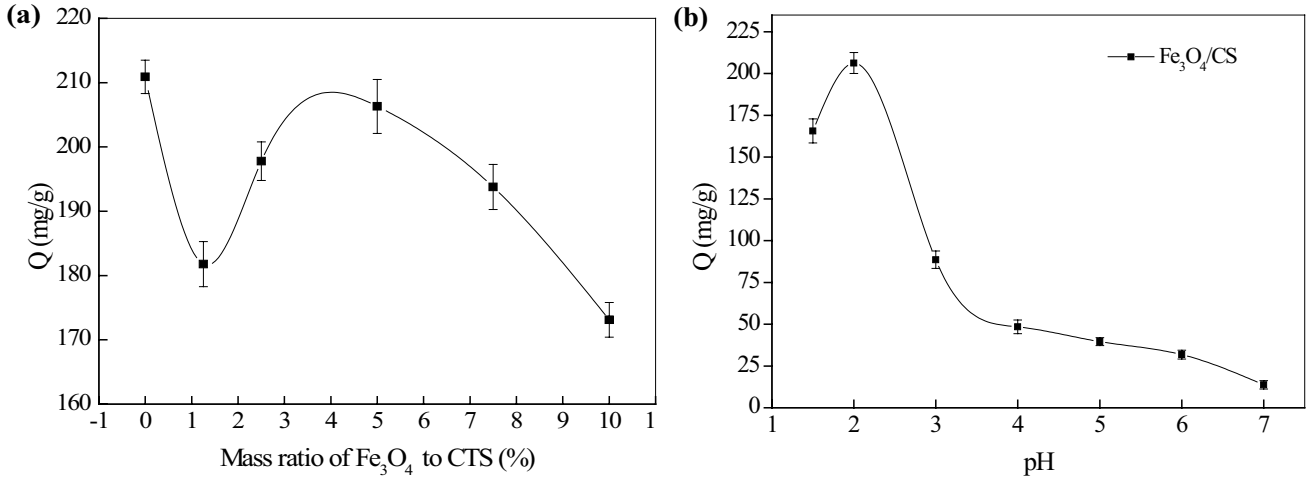

Fig. 5. Effect of the Fe_3O_4/chitosan ratio (a) and pH (b) on adsorption capacity.

top, the value drops gradually. It could be seen clearly that the vertex of the curve reached at the Fe_3O_4/chitosan ratio 0.2:4 (g/g), and the adsorption capacity of sulfate was 206.30 mg g^{-1}. By introducing Fe_3O_4 powders into chitosan microspheres, the mass of the adsorbent increased per mass while the adsorptive sites decreased, which lead to decrease in adsorption capacity at first. With the increase of Fe_3O_4, the magnetic particles can be well dispersed in an appropriate proportion, which may increase the adsorption capacity. Due to the –OH and $–NH_2$ can be coordinated with Fe_3O_4, the excessive magnetic particles will reduce the content of functional groups in a certain extent, resulting in a loss of adsorption capacity. In conclusion, 0.2:4 (g/g) could be regarded as the optimal mass ratio of Fe_3O_4 and chitosan.

3.2.2. Effect of pH

The effect of pH on the sulfate sorption was determined at seven different pH levels on Fe_3O_4/CS, and 0.1 mol L^{-1} HCl or NaOH solutions were used to adjust the initial pH values ranging from 1.5 to 7.0. The initial concentration of the sulfate aqueous solution was 600 mg L^{-1}, and 0.05 g magnetic chitosan powder were weighed and added into the solutions at different pH values under oscillating at 303.15 K for 3 h. As shown in Fig. 5b, pH had a great influence on the adsorption capacity of Fe_3O_4/CS. The maximum adsorption capacity of sulfate on Fe_3O_4/CS reached 206.30 mg g^{-1} at pH 2.0.

The high adsorption capacity at low pH is mainly due to strong electrostatic interaction between the positively charged sites of adsorbent and the sulfate anion. The $–NH_2$ of chitosan are protonated in the highly acidic environment, which will enhance the electrostatic attraction of anions, further increasing the adsorption capacity of sulfate. However, chitosan will degrade and its adsorbability will decrease when the pH is less than 2.0. When the pH of the solution increases, the surface becomes negatively charged and the electrostatic repulsion enhanced. Then the negatively charged surface sites on the adsorbent exclude sulfate, resulting in the sharp decrease of the adsorption amount for sulfate [23].

3.2.3. Effect of contact time

The adsorption capacity of Fe_3O_4/CS for the removal of sulfate was determined by varying the contact time in the range of 20–360 min at 0.05 g adsorbent dose with 600 mg L^{-1} sulfate solution in pH 2.0 at 303.15 K. The samples were taken out at different time and the concentration were determined. As shown in Fig. 6a, the adsorbent reached saturation at 120 min, and thereafter remained almost constant. Initially, the adsorption proceeded quickly, possibly due to a greater availability of binding sites over the adsorbent surface. After a time, the remaining vacant surface sites were difficult to be occupied due to repulsive forces between sulfate adsorbed on the surface of adsorbents and solution phase. However, there was some decrease after 300 min, which may be due to the desorption behaviors. The maximal sulfate uptake by Fe_3O_4/CS was 206.48 mg g^{-1}. To achieve adsorption equilibrium, a 180 min contact time was selected in the study.

3.2.4. Effect of initial concentration of sulfate

The effect of initial concentration of sulfate on adsorption capacity was carried out by vibrating 50 mL different concentration of sulfate aqueous solution at pH 2.0, which was added with 0.05 g adsorbents under oscillating at 303.15 K for a contact time of 180 min. The results were represented in graphical form as adsorption capacity vs. initial sulfate concentration in Fig. 6b. It is observed from Fig. 6b that the Q of sulfate increased from 46.39 to 206.39 mg g^{-1} with the increase in initial sulfate concentration ranging from 100 to 1,000 mg L^{-1}. The results illustrated that high concentration gradient acting as a driving force overcame mass transfer resistance between bulk solution and adsorbent surface [24]. Initially, the adsorption capacity had maintained a sustained, rapid upward trend and thereafter remained almost constant. This may due to the fact that almost all the molecules were adsorbed very quickly on the outer surface at lower concentrations. However, further increases in initial concentrations led to fast saturation of adsorbent surface, and thus most of the sulfate ions adsorption took place slowly inside the pores [25].

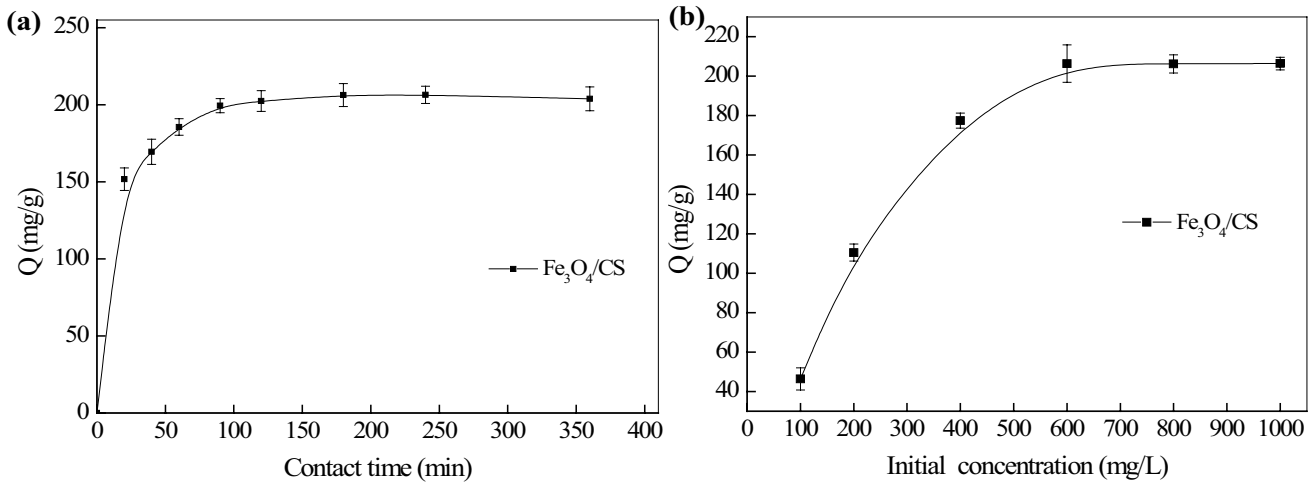

Fig. 6. Effect of contact time (a) and initial concentration (b) on adsorption capacity.

3.2.5. Effect of adsorbent dosage

Adsorbent dosage was a vital parameter influencing adsorption capacity and effluent concentration. To investigate the effect of adsorbent dosage on sulfate adsorption, different dosages of adsorbents were placed in 600 mg L^{-1} sulfate solution in pH 2.0 at 303.15 K for 3 h. The result is shown in Fig. 7a. It was evident that the Q of sulfate decreased with the increase in adsorbent dosage from 0.2 to 4.0 g L^{-1}, and the removal rate increased sharply initially and eventually was stabilized at about 62%. The result indicated that the number of active sites and the adsorption surface area increased with an increase of adsorbent dose, which obviously enhanced the removal rate of sulfate. As shown in Fig. 7a, further increase in dosage beyond 3 g L^{-1} rarely affected adsorption capacity of adsorbent.

3.2.6. Effect of co-existing ions

As the necessary nutrients for biological organisms, nitrate and phosphate are present in all natural water. They may compete with sulfate for the active sites on the surface of the adsorbents during the adsorption process. In order to examine their influence on the adsorption of Fe_3O_4/CS for the removal of sulfate, various concentrations of nitrate and phosphate were added to the sulfate solution. The initial concentration of sulfate was 600 mg L^{-1} at pH 2.0, and the experiment was carried out with 0.05 g adsorbents at 303.15 K for 3 h. As shown in Fig. 7b, the presence of other ions decreased the adsorption capacity of sulfate. The higher the concentration of coexisting ions, the greater the reduction. The anions reduced the sulfate adsorption on Fe_3O_4/CS in the order of $PO_4^{3-} + NO_3^- > PO_4^{3-} > NO_3^-$, suggesting that those anions could enhance the Coulombic repulsion forces and compete with sulfate for the active sites, readily decreasing the adsorption capacity of sulfate.

3.3. Adsorption kinetics

Adsorption kinetics is one of the most important characteristics which represent the adsorption efficiency. Therefore, three kinetic order models were studied to fit the experimental data: the pseudo-first-order, the pseudo-second-order and the intraparticle diffusion model [26,27].

The pseudo-first-order kinetic model is expressed as follows:

$$Q_t = Q_e\left(1 - e^{-k_3 t}\right) \tag{4}$$

where Q_e (mg g^{-1}) and Q_t (mg g^{-1}) are the adsorption capacities of the adsorbate at equilibrium and at any time t, respectively, and k_3 (min^{-1}) is the rate constant of first-order sorption, which can be calculated from the plot of Q_t against t.

The pseudo-second-order kinetic model is expressed as follows:

$$Q_t = \frac{k_4 Q_e^2 t}{1 + k_4 Q_e t} \tag{5}$$

where k_4 (g min^{-1} mg^{-1}) is the rate constant of second-order sorption, and the Q_e as well as k_4 can be obtained from the non-linear plot of Q_t against t.

The intraparticle diffusion models can be obtained from Weber–Morris equation as follows:

$$Q_t = k_p t^{1/2} + C \tag{6}$$

where k_p (mg $min^{-0.5}$ g^{-1}) is the intraparticle diffusion rate constant.

The non-linear fitting figures of pseudo-first-order, second-order models are shown in Figs. 8a and b, respectively. Based on the data in Fig. 9, the related parameters of the kinetic models can be calculated. They are shown in Table 2. By comparing the values of the correlation coefficients R^2, it could be seen that the pseudo-second-order mechanism rather than the pseudo-first-order mechanism conforms to the sulfate adsorption processes on Fe_3O_4/CS, which indicates that the chemisorptions might be the rate-limiting step that controls the adsorption processes.

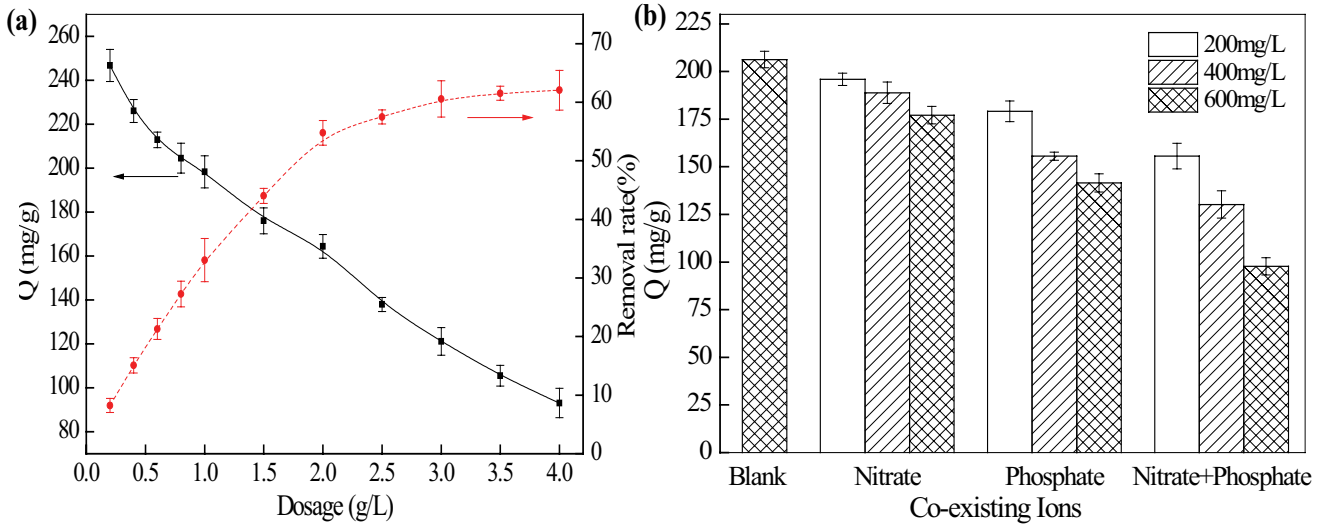

Fig. 7. Effect of adsorbent dosage (a) and co-existing ions (b) on adsorption capacity.

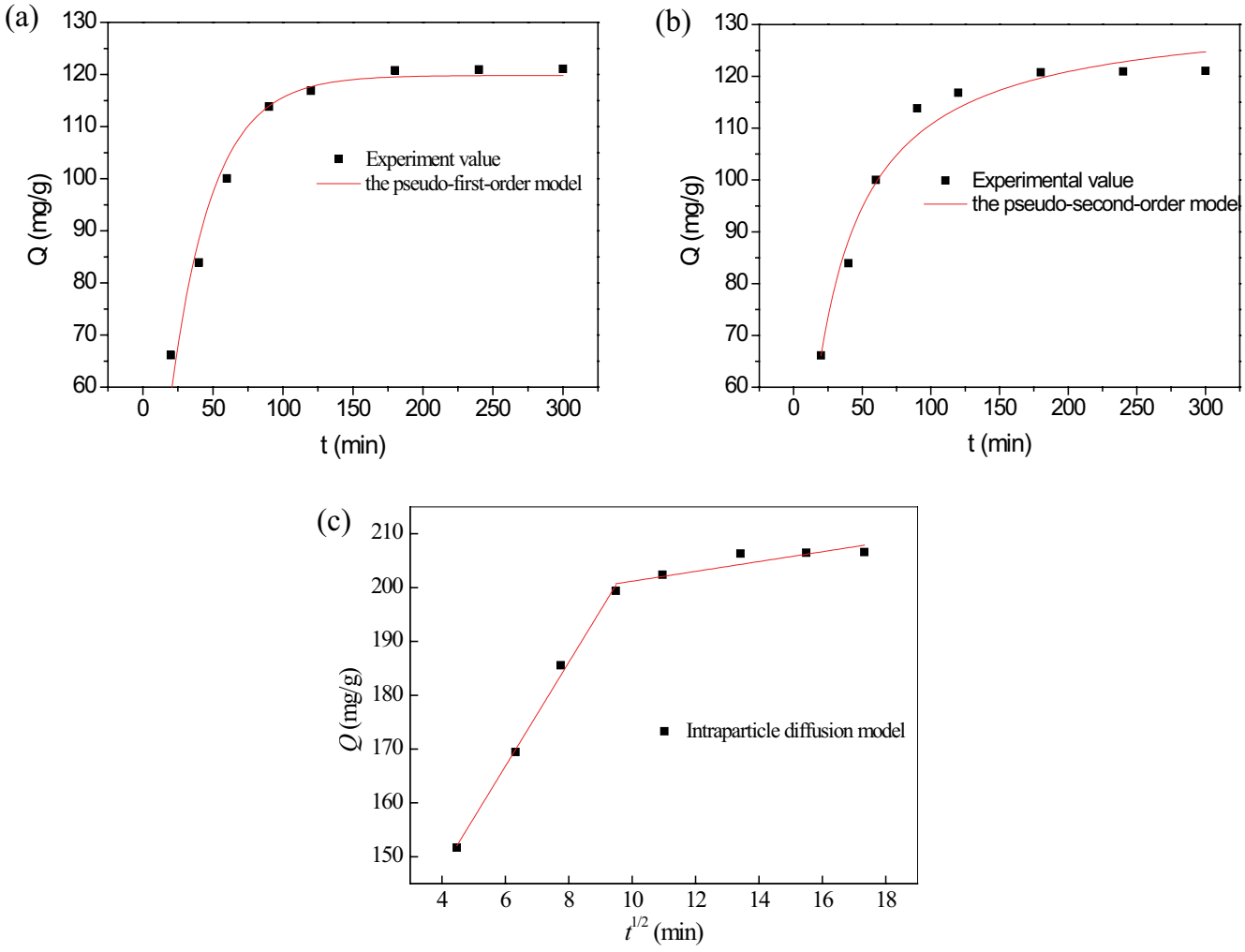

Fig. 8. Pseudo-first-order and pseudo-second-order kinetics (a), and the intraparticle diffusion model (b) for sulfate sorption on Fe_3O_4/CS.

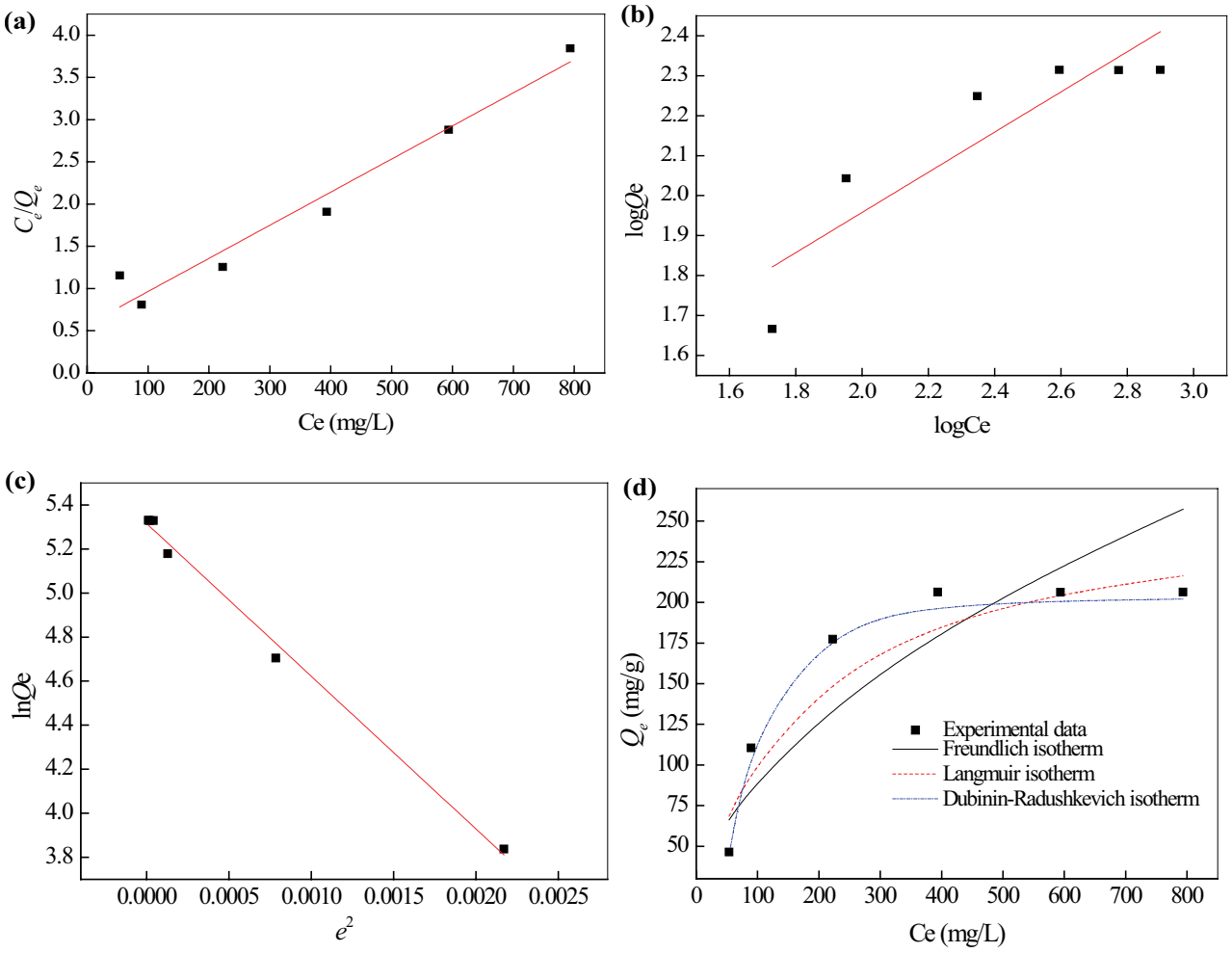

Fig. 9. Adsorption isotherms for sulfate sorption: Langmuir isotherm (a), Freundlich isotherm (b), Dubinin–Radushkevich isotherm (c) and equilibrium adsorption model (d).

The fitting figures of pseudo first-order, second-order models and intraparticle diffusion models are shown in Fig. 8. The related parameters of the kinetic models can be calculated from the data in Fig. 8. They are shown in Table 1. By comparing the values of the linear correlation coefficients R^2, it could be seen that the pseudo-second-order mechanism rather than the pseudo-first-order mechanism conformed to the sulfate adsorption processes on Fe_3O_4/CS. As we can see from Fig. 8c, the adsorption process was divided into two phases, including a fast adsorption phase on the surface of the adsorbent and a slow pore diffusion phase. In addition, we can see the fitted curves did not pass through the origin point, which indicates that the intraparticle diffusion is not the only limiting step during the adsorption process.

3.4. Adsorption isotherms

3.4.1. Langmuir isotherm

The Langmuir isotherm model is based on the assumption of a structurally homogeneous adsorbent that all adsorption sites are identical and energetically equivalent [28], and there

Table 1
Adsorption parameters of kinetic models for sulfate sorption on Fe_3O_4/CS

Pseudo-first-order kinetic models			Pseudo-second-order kinetic models			Intraparticle diffusion models			
Q_e (mg g^{-1})	k_1 (min^{-1})	R^2	Q_e (mg g^{-1})	k_2 (g min^{-1} mg^{-1})	R^2	k_{p1} (mg min$^{-0.5}$ g^{-1})	R^2	k_{p2} (mg min$^{-0.5}$ g^{-1})	R^2
119.81	0.0334	0.9614	133.18	3.6998×10^{-4}	0.9710	9.6553	0.9959	0.9135	0.8184

is no interaction amidst the adsorbed molecules. Therefore, the Langmuir isotherm is often used for the fitting of a monolayer adsorption.

The non-linearized and linearized form of Langmuir isotherm can be described by the following equations:

$$Q_e = \frac{Q_{\max} b C_e}{1 + b C_e} \tag{7}$$

$$\frac{C_e}{Q_e} = \frac{C_e}{Q_{\max}} + \frac{1}{Q_{\max} b} \tag{8}$$

where Q_{max} (mg g^{-1}) represents the maximum adsorption capacity, C_e (mg L^{-1}) is the concentration of sulfate in the aqueous solution at equilibrium, b is the Langmuir constant related to the affinity of the binding sites.

3.4.2. Freundlich isotherm

Compared with the Langmuir isotherm model, the Freundlich isotherm can be applied to multilayer adsorption and there is interaction amidst the adsorbed molecules, which are the main differences between them.

The non-linearized and linearized form of Langmuir isotherm can be described by the following equations [29]:

$$Q_e = k C_e^{1/n} + C \tag{9}$$

$$\log Q_e = \log k + \frac{1}{n} \log C_e \tag{10}$$

where k is the Freundlich constant related to the adsorption capacity, $1/n$ is the Freundlich constant related to the adsorption intensity, C is constant.

3.4.3. Dubinin–Radushkevich isotherm

The Dubinin–Radushkevich (DR) equation is widely used for describing the adsorption in microporous materials. It is based on the assumption that the characteristic sorption curve is related to the porous structure of the sorbent and apparent energy of adsorption [30]. The DR model is applied to distinguish the physical and chemical adsorption of sulfate. The non-linearized and linearized forms are as follows:

$$Q_e = Q_{\max} \exp\left(-Be^2\right) \tag{11}$$

$$\ln Q_e = \ln Q_{\max} - Be^2 \tag{12}$$

where B (mol^2 kJ^{-2}) is a constant related to the free energy of sorption, e is the Polanyi potential, equal to $RT\ln(1 + 1/C_e)$, R is the ideal gas constant, 8.314 × 10^{-3} kJ mol^{-1} K^{-1}, T (K) is the thermodynamic temperature. B and Q_{max} can be obtained from the slope and the intercept in Fig. 9c, respectively.

The constant B gives the mean free energy E (kJ mol^{-1}) of adsorption per molecule of the adsorbate when it is transferred from the solid from infinity in the solution [31] and the relation is given as follows:

$$E = \frac{1}{\sqrt{2B}} \tag{13}$$

The fitting figures of the isotherm models are shown in Fig. 9. Table 2 shows the calculated values of Langmuir, Freundlich and Dubinin–Radushkevich models' parameters. It can be seen from Table 2 that the R^2 of Langmuir isotherm is much higher than that of Freundlich isotherm, which indicates that the sulfate ions are mainly adsorbed in monolayer coverage manner without interaction amidst the adsorbed ions. It is hence considered that the values of Q_{max} deduced from the Langmuir model could show the adsorption ability of the composite. From the Langmuir models, it can be concluded that the maximum adsorption capacity at 303.15 K of Fe_3O_4/CS is 256.41 mg g^{-1}.

As shown in Fig. 9d, both Langmuir isothermal model and Dubinin–Radushkevich isothermal model are close to the experimental data. Therefore, the Langmuir isothermal model can be commendably instead of DR isothermal model. From the DR isotherm, the calculated values of E can be obtained and used to determine the chemical or physical properties of the sorption. If the value of E is lower than 8 kJ mol^{-1}, the adsorption process is of a physical nature [32]. It can be seen that the calculated mean energy value of adsorption of the sulfate by Fe_3O_4/CS is very small (0.0269 kJ mol^{-1}), indicating the type of adsorption appears to be the physical adsorption. The Q_{max} values of various materials for the adsorption of sulfate from aqueous solution as reported in the literature are listed in Table 3. We observed that the Q_{max} values varied considerably for different adsorbents. The cross-linked Fe_3O_4/CS has a better adsorption effect on sulfate from aqueous solution.

3.5. Setting performance of the Fe_3O_4/CS

In order to verify whether the Fe_3O_4/CS can be easily and simply separated using the external magnetic field, a simple experiment was carried out. In two standard measuring cylinders, 50 mL deionized water and 0.5 g magnetic chitosan powder were added in order, respectively. After fast shaking,

Table 2
Adsorption parameters of isotherms for sulfate sorption on Fe_3O_4/CS

Langmuir isotherm			Freundlich isotherm			Dubinin–Radushkevich isotherm			
Q_{max} (mg g^{-1})	B	R^2	$1/n$	K (L g^{-1})	R^2	Q_{max} (mg g^{-1})	B (mol^2 kJ^{-2})	E (kJ mol^{-1})	R^2
256.41	0.0068	0.9625	0.5030	8.952	0.8121	203.446	693.26	0.0269	0.9942

Table 3
Q_{max} values of various materials for the adsorption of sulfate from aqueous solution as reported in the literature

Adsorbent	Concentration of sulfate (mg L^{-1})	Q_{max} (mg g^{-1})	Reference
Magnetic chitosan (Fe_3O_4/CS)	100–1,000	256.41	This study
Granular ferric hydroxide	50–800	44.64	[10]
Modified rice straw	50–500	74.76	[4]
Organo-nano-clay	25–500	38.02	[5]
Filter sand	20–2,000	285	[6]
Iron sand	20–2,000	11.37	
Modified sugarcane bagasse cellulose	71–710	56.8	[12]

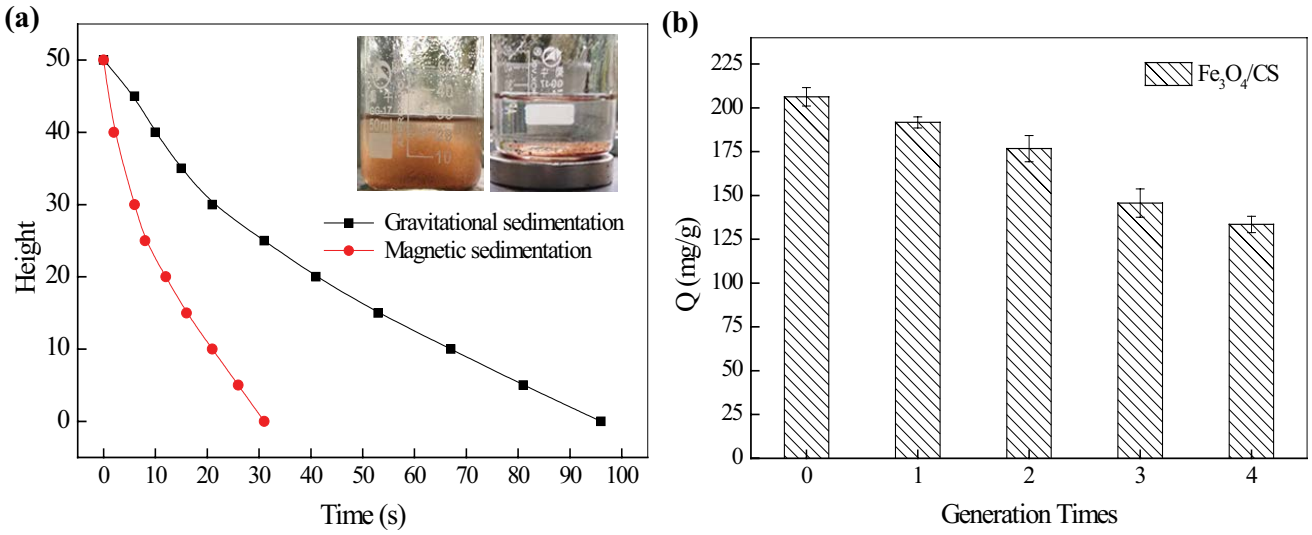

Fig. 10. Effect of magnetic field on setting time of Fe_3O_4/CS (a) and the generation times on adsorption capacity (b).

one of the measuring cylinders was put on a magnet. Keeping the bottom of the two measuring cylinders at the same level, the changes of location is recorded in Fig. 10a.

As shown in Fig. 10a, Fe_3O_4/CS could be rapidly settled in 30 s, while the gravitational sedimentation process takes 96 s. Obviously, it will greatly save separation recovery time. Besides, the particles could be easily lost during the gravitational sedimentation process, resulting in the reduction of the recovery rate. Therefore, most of the magnetic chitosan particles could be rapidly collected in a magnetic field, which will be conducive to improve the reusability of Fe_3O_4/CS.

3.6. Regeneration studies

High adsorption capacity and good reusability were of the utmost importance for any adsorbent, which would significantly lower the cost and promote economic value of adsorption method. Thus, the regeneration and reuse experiments were investigated in the study. 0.1 mol L^{-1} NaOH solutions were used to treat the adsorbents which had adsorbed sulfate for the removal of sulfate. After washed with distilled water for three times, the adsorbed adsorbents were added to the sodium hydroxide solution. Then the mixture was agitated at 303.15 K for 24 h followed by filtration. The wet adsorbents were washed repeatedly with distilled water until it became neutral. Finally, the regenerated adsorbents were used to re-adsorb the sulfate anions. Repeating the experiment four times, the changes of its adsorption capacity are shown in Fig. 10b. As can be seen in Fig. 10b, with the increase in the number of regeneration, the adsorption capacity of sulfate on Fe_3O_4/CS decreased from 191.72 to 133.48 mg g^{-1}. It was shown that the loss of adsorption capacity ranged from 7% to 30%, indicating that Fe_3O_4/CS had a good performance on regeneration. Besides, the total adsorption capacity of sulfate sorption can reach 849.88 mg g^{-1}, further demonstrating its good reusability.

4. Conclusions

This study shows that the cross-linked magnetic chitosan (Fe_3O_4/CS) is an effective adsorbent for the removal of sulfate from aqueous solution. According to characterization analyses, Fe_3O_4/CS was successfully synthesized. Different parameters were studied to investigate the sulfate sorption capabilities of Fe_3O_4/CS. Based on the batch adsorption studies, it can be concluded that the optimization conditions of adsorption sulfate ions onto Fe_3O_4/CS was that the Fe_3O_4/chitosan ratio was 0.2:4 (g/g), the pH value was 2.0, the

equilibrium time was 180 min, and the adsorbent dosage was 3 g L^{-1}. The equilibrium data fit Langmuir isothermal model well, while the adsorption process can be well described by the second-order kinetic model. In addition, the Dubinin–Radushkevich isotherm confirmed the presence of physical adsorption forces. Based on the Langmuir isotherm model, the maximum adsorption capacity on Fe_3O_4/CS was 256.41 mg g^{-1}. The chitosan composites could be reused when an alkaline solution was used as a regenerant, which had a good performance on regeneration and reuse. Besides, Fe_3O_4/CS can be easily and simply separated using the external magnetic field. Overall, this study illustrated that Fe_3O_4/CS was a promising material for the removal of sulfate from aqueous solution.

Acknowledgments

This work was supported by National Natural Science Foundation of China (50904047; 41501537); Science and Technology Department of Hubei Provincial (2016CFA086).

References

[1] W. Dou, Z. Zhou, L.M. Jiang, A.J. Jiang, R.W. Huang, X.C. Tian, W. Zhang, D.Q. Chen, Sulfate removal from wastewater using ettringite precipitation: magnesium ion inhibition and process optimization, J. Environ. Manage., 196 (2017) 518–526.
[2] K. Wang, Y.X. Sheng, H.B. Cao, K.P. Yan, Y. Zhang, Impact of applied current on sulfate-rich wastewater treatment and microbial biodiversity in the cathode chamber of microbial electrolysis cell (MEC) reactor, Chem. Eng. J., 307 (2017) 150–158.
[3] A. Silambarasan, P. Rajesh, P. Ramasamy, Growth kinetics and bulk growth of inversely soluble lithium sulfate monohydrate single crystals and their characterization, J. Cryst. Growth, 468 (2017) 38–42.
[4] W. Cao, Z. Dang, X.-Q. Zhou, X.-Y. Yia, P.-X. Wu, N.-W. Zhu, G.-N. Lu, Removal of sulphate from aqueous solution using modified rice straw: preparation, characterization and adsorption performance, Carbohydr. Polym., 85 (2011) 571–577.
[5] W. Chen, H.-C. Liu, Adsorption of sulfate in aqueous solutions by organo-nano-clay: adsorption equilibrium and kinetic studies, J. Central South Univ., 21 (2014) 1974–1981.
[6] E. Iakovleva, E. Makila, J. Salonen, M. Sitarz, M. Sillanpaa, Industrial products and wastes as adsorbents for sulphate and chloride removal from synthetic alkaline solution and mine process water, Chem. Eng. J., 259 (2015) 364–371.
[7] E.Y. Jo, S.M. Park, I.S. Yeo, J.D. Cha, J.Y. Lee, Y.H. Kim, T.K. Lee, C.G. Park, A study on the removal of sulfate and nitrate from the wet scrubber wastewater using electrocoagulation, Desal. Wat. Treat., 57 (2016) 7833–7840.
[8] P.H.A. Timmers, D.A. Suarez-Zuluaga, M. van Rossem, M. Diender, A.J.M. Stams, C.M. Plugge, Anaerobic oxidation of methane associated with sulfate reduction in a natural freshwater gas source, ISME J., 10 (2016) 1400–1412.
[9] J. Liu, X. Yue, Y. Yang, Y. Guo, Adsorption of sulfate from natural water on calcined Mg-Fe layered double hydroxides, Desal. Wat. Treat., 56 (2015) 274–283.
[10] M. Shams, M. Qasemi, M. Afsharnia, A.H. Mahvi, Sulphate removal from aqueous solutions by granular ferric hydroxide, Desal. Wat. Treat., 57 (2016) 23800–23807.
[11] R. Dong, Y.F. Liu, X.G. Wang, J.H. Huang, Adsorption of sulfate ions from aqueous solution by surfactant-modified palygorskite, J. Chem. Eng. Data, 56 (2011) 3890–3896.
[12] D.R. Mulinari, M.L.C.P. da Silva, Adsorption of sulphate ions by modification of sugarcane bagasse cellulose, Carbohydr. Polym., 74 (2008) 617–620.
[13] R. Yang, H. Li, M. Huang, H. Yang, A. Li, A review on chitosan-based flocculants and their applications in water treatment, Water Res., 95 (2016) 59–89.
[14] R. Yang, D. Li, A. Li, H. Yang, Adsorption properties and mechanisms of palygorskite for removal of various ionic dyes from water, Appl. Clay Sci., 151 (2018) 20–28.
[15] Y. Xie, S. Li, G. Liu, J. Wang, K. Wu, Equilibrium, kinetic and thermodynamic studies on perchlorate adsorption by cross-linked quaternary chitosan, Chem. Eng. J., 192 (2012) 269–275.
[16] T.T. Zhao, T. Feng, Application of modified chitosan microspheres for nitrate and phosphate adsorption from aqueous solution, RSC Adv., 6 (2016) 90878–90886.
[17] P. Miretzky, A.F. Cirelli, Fluoride removal from water by chitosan derivatives and composites: a review, J. Fluorine Chem., 132 (2011) 231–240.
[18] J.X. Li, B.Q. Jiang, Y. Liu, C.Q. Qiu, J.J. Hu, G.R. Qian, W.S. Guo, H.H. Ngo, Preparation and adsorption properties of magnetic chitosan composite adsorbent for Cu^{2+} removal, J. Cleaner Prod., 158 (2017) 51–58.
[19] K. Li, P. Li, J. Cai, S. Xiao, H. Yang, A. Li, Efficient adsorption of both methyl orange and chromium from their aqueous mixtures using a quaternary ammonium salt modified chitosan magnetic composite adsorbent, Chemosphere, 154 (2016) 310–318.
[20] X.D. Zhao, Q.M. Feng, W.Q. Wang, Preparation and surface modification of magnetic nano-Fe_3O_4, Appl. Chem. Ind., 39 (2010) 171–174.
[21] M. Ghaedi, S. Hajjati, Z. Mahmudi, I. Tyagi, S. Agarwal, A. Maity, V.K. Gupta, Modeling of Competitive ultrasonic assisted removal of the dyes - Methylene blue and Safranin-O using Fe_3O_4 nanoparticles, Chem. Eng. J., 268 (2015) 28–37.
[22] K.L. Huang, J. Chen, S. Liu, G. Li, Chemical modification and coating mechanism of magnetic Fe_3O_4/chitosan, Chin. J. Inorg. Chem., 23 (2007) 1491–1495.
[23] Y. Çengeloğlu, A. Torb, M. Ersoza, G. Arslan, Removal of nitrate from aqueous solution by using red mud, Sep. Purif. Technol., 51 (2006) 374–378.
[24] Q. Hu, N. Chen, C. Feng, W.W. Hu, Nitrate adsorption from aqueous solution using granular chitosan-Fe^{3+} complex, Appl. Surf. Sci., 347 (2015) 1–9.
[25] C.K. Geethamani, S.T. Ramesh, R. Gandhimathi, P.V. Nidheesh, Alkali-treated fly ash for the removal of fluoride from aqueous solutions, Desal. Wat. Treat., 52 (2014) 3466–3476.
[26] Y.S. Ho, G. Mckay, Pseudo-second order model for sorption processes, Process Biochem., 34 (1999) 451–465.
[27] L. Largitte, R. Pasquier, A review of the kinetics adsorption models and their application to the adsorption of lead by an activated carbon, Chem. Eng. Res. Des., 109 (2016) 495–504.
[28] T. Feng, S. Xiong, F. Zhang, Application of cross-linked porous chitosan films for Congo red adsorption from aqueous solution, Desal. Wat. Treat., 53 (2013) 1970–1976.
[29] Y.S. Ho, Isotherms for the sorption of lead onto peat: comparison of linear and non-linear methods, Pol. J. Environ. Stud., 53 (2006) 996–1009.
[30] S. Vasudevan, J. Lakshmi, The adsorption of phosphate by graphene from aqueous solution, RSC Adv., 2 (2012) 5234–5242.
[31] M.H. Dehghani, G.A. Haghighat, K. Yetilmezsoy, G. McKay, B. Heibati, L. Tyagi, S. Agarwal, V.K. Gupta, Adsorptive removal of fluoride from aqueous solution using single- and multi-walled carbon nanotubes, J. Mol. Liq., 216 (2016) 401–410.
[32] V. Srihari, A. Das, Comparative studies on adsorptive removal of phenol by three agro-based carbons: equilibrium and isotherm studies, Ecotoxicol. Environ. Saf., 71 (2008) 274–283.